Eur. Phys. J. D **35**, 177–191 (2005)
DOI: 10.1140/epjd/e2005-00230-6

THE EUROPEAN PHYSICAL JOURNAL D

High resolution study of anion formation in low-energy electron attachment to SF_6 molecules in a seeded supersonic beam

M. Braun, S. Barsotti, S. Marienfeld, E. Leber, J.M. Weber, M.-W. Ruf, and H. Hotop[a]

Fachbereich Physik, Technische Universität, 67653 Kaiserslautern, Germany

Received 14 April 2005
Published online 17 August 2005 –

Abstract. Using two variants of the Laser Photoelectron Attachment (LPA) method involving a differentially-pumped, seeded supersonic beam (0.05% and 12.5% of SF_6 molecules in helium carrier gas, nozzle temperatures T_0 = 300–600 K, stagnation pressures p_0 = 1–5 bar) and mass spectrometric ion detection, we have investigated the energy dependence of anion formation in low-energy electron collisions with SF_6 molecules at high energy resolution. Using the standard LPA method, the yield for SF_6^- as well as SF_5^- and F^- anions was studied with an energy width around 1 meV over the electron energy range 0–200 meV. In addition, a variant of the LPA method with extended energy range (denoted as EXLPA) was developed and applied to measure the yield for SF_6^- and SF_5^- formation over the energy range 0–1.5 eV with an energy width of about 20 meV. The cross-section for formation of SF_6^- decreases by five orders of magnitude over the range 1–500 meV and is only weakly dependent on nozzle temperature. The yield for SF_5^- formation shows — apart from a weak zero energy peak which grows strongly with rising temperature — a broad maximum (located around 0.6 eV for $T_0 = 300$ K and shifting to lower energies with rising T_0) and a monotonical decrease towards higher energies. SF_5^- attachment spectra taken at elevated temperatures exhibit changes with rising stagnation pressure which directly reflect rovibrational cooling of the SF_6 molecules with rising pressure. The SF_5^-/SF_6^- intensity ratio at near-zero energy and the low-energy shape of the broad peak in the SF_5^- spectra are used as thermometers for the internal temperature of the SF_6 molecules in the seeded supersonic beam which (at $p_0 = 1$ bar) are found to be 50–100 K lower than the nozzle temperature. The energy dependence of the yield for F^- formation is similar to that for SF_6^-, but the F^- signals are three to four orders of magnitude lower than those for SF_6^-; in view of the rather high endothermicity of F^- formation the origin of the F^- signals is discussed in some detail.

PACS. 34.80.Lx Electron-ion recombination and electron attachment – 34.80.Ht Dissociation and dissociative attachment by electron impact

1 Introduction

Negative ion formation in low-energy electron attachment to SF_6 molecules

$$e^-(E) + SF_6 \rightarrow [SF_6^-] \rightarrow \text{ negative ions} \qquad (1)$$

is an important process in gaseous dielectrics and has been studied for a long time [1,2]. Near zero electron energy E, metastable SF_6^- ions are formed by s-wave attachment with a $E^{-1/2}$ behaviour of the cross-section [3–9] which reaches a value of 2×10^{-17} m^2 at E = 1 meV [2,5,9]. Towards higher energies, dissociative electron attachment (DEA) yielding SF_5^- ions takes over with a peak maximum which is located at several tenths of an eV [2,10–17]. The shape of this DEA cross-section was found to be strongly dependent on the temperature T_i (i.e. internal rovibrational energy) of the SF_6 target molecules, exhibiting a shift and a rise of the peak cross-section towards zero energy with increasing T_i [2,12,16]. At electron energies above about 2 eV, other fragment anions including F^-, F_2^-, and SF_4^- are formed through several repulsive resonances [2,18].

In spite of these various efforts, important questions remained open, partly due to inconsistent experimental observations:

(i) Why do different experiments yield widely different lifetimes of the metastable SF_6^- ion, ranging from several μs to several ms [19–33]?
(ii) To what extent does autodetachment of the SF_6^- ion influence the experimentally observed anion yield $Y(SF_6^-)$ and thus the intensity ratios $R = Y(SF_5^-)/Y(SF_6^-)$ as a function of electron energy and gas temperature T_i of the SF_6 target molecules?
(iii) What is the threshold behaviour of the DEA process yielding SF_5^- ions when viewed with meV resolution?

[a] e-mail: hotop@physik.uni.kl.de

At which energy does the maximum yield for this channel occur at room temperature?

(iv) Does dissociative electron attachment proceed through two different anion potential surfaces at energies below 1.5 eV?

(v) To what extent does F^- formation occur at near zero electron energies?

With the aim to shed new light on some of these questions, we apply the Laser Photoelectron Attachment (LPA) method, involving a differentially-pumped supersonic beam of SF_6 molecules seeded in helium carrier gas (nozzle temperature $T_0 = 300$–600 K) and mass spectrometric anion detection, to provide highly resolved cross-sections for SF_6^- as well as for SF_5^- and F^- formation over the range 0–200 meV at meV energy width. In addition, we use a novel variant of the LPA method (denoted as EXLPA) to measure the yield for SF_6^- and SF_5^- formation over the extended energy range 0–1.5 eV with an energy width of about 20 meV. In this EXLPA approach, essentially zero energy photoelectrons are created in a separate photoionization chamber, accelerated to variable energies and magnetically guided to the electrically field-free attachment region of the collimated target beam. In Section 2, we describe the experimental set-up and procedures. In Section 3, we present the results of test measurements and we report attachment spectra, obtained at several nozzle temperatures and stagnation pressures over extended electron energy ranges; moreover, we will discuss the findings in comparison with previous work. We conclude in Section 4 with a brief summary.

2 Experimental

2.1 Standard laser photoelectron attachment (LPA) method

In the present work we use two different variants of the Laser Photoelectron Attachment (LPA) method, as illustrated in Figure 1 with the lasers arranged for EXLPA operation. In the standard LPA approach [5,34–36] energy-variable, monoenergetic electrons, created by photoionization of atoms in a collimated beam, interact with the target molecules of interest in the region where the photoionization process takes place (center of reaction chamber RC). Negative ions due to electron attachment reactions are detected with a quadrupole mass spectrometer.

In the present LPA work, photoelectrons (current 20 pA) are produced by two-step photoionization of potassium atoms [36–38]. Both hyperfine components of ground state $^{39}K(4s,\ F = 1, 2)$ atoms in a collimated beam (collimation 1:400, diameter 1.5 mm) from a doubly differentially pumped metal vapour oven are transversely excited to the $^{39}K^*(4p_{3/2},\ F = 2, 3)$ states by the first sidebands of the electro-optically modulated (frequency 220.35 MHz) output of a long-term stabilized single mode cw titanium: sapphire laser ($\lambda_1 = 766.7$ nm) [38]. Part of the excited state population is transferred to high Rydberg levels (nd, $(n+2)s$, $n \geq 12$) or photoionized by interaction with the intracavity field of a multimode tunable dye laser (bandwidth 40 GHz, power up to 5 W), operated in the blue spectral region ($\lambda_2 = 472-424$ nm, dye stilbene 3). The energy of the photoelectrons is continuously varied over the range 0–200 meV by tuning the wavelength of the ionizing laser ($\lambda_2 < 455$ nm). At wavelengths above 455 nm, $^{39}K^{**}(ns, nd)$ Rydberg atoms are produced which can be used to study Rydberg electron transfer (RET) reactions of the type

$$K^{**}(nl) + SF_6 \rightarrow K^+ + \text{anions}. \qquad (2)$$

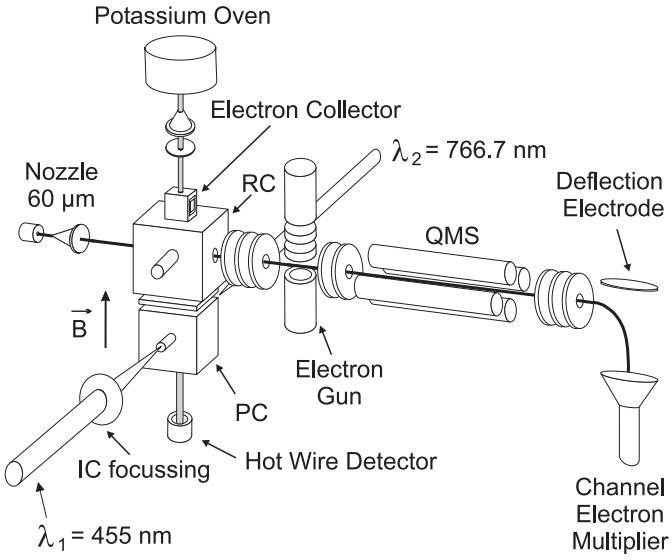

Fig. 1. Experimental set-up for LPA and EXLPA measurements (the lasers are arranged for EXLPA operation; in the standard LPA approach, the lasers are shifted upwards and directed — without focussing – through the center of RC).

Electrons, created in the overlap volume of the potassium atom beam and the laser beams, may attach to molecules in a collimated, differentially pumped, seeded supersonic beam (0.05% or 12.5% SF_6 in helium; diameter in the reaction region 3 mm; nozzle diameter $d_0 = 60$ μm, stagnation pressure $p_0 = 1$–5 bar, nozzle temperature $T_0 = 300$–600 K), propagating in a direction perpendicular to both the potassium and the laser beams. Anions, generated by electron attachment and drifting out of the essentially field free reaction chamber, are imaged into a quadrupole mass spectrometer ($m/q \leq 2000$ u/e) with a combination of two electrostatic lenses (see Fig. 1). The ion optics are carefully tuned for optimum detection of the ion of interest. The transmitted ions are accelerated to an energy of 1 keV and detected by a differentially pumped off-axis ceramic channel electron multiplier (Sjuts) with low background (<0.02 s^{-1}).

For diagnostics of the target beam (especially with respect to possible cluster formation and the detection of impurity species), positive ion mass spectra can be generated by electron impact ionization with an auxiliary electron gun (see Fig. 1; current around 0.1–1 μA, energy 70–85 eV). The He/SF_6 gas for the present work was

supplied by Messer Griesheim GmbH with a stated purity of 99.996% (He grade 4.6) and 99.9% (SF_6 grade 3.0), respectively.

The reaction volume is surrounded by a cubic chamber made of oxygen free, high conductivity copper, the inner walls of which are coated with colloidal graphite. By applying bias potentials to each face of the cube, dc stray electric fields are reduced to values $F_S < 0.2$ V m^{-1} (see below). Magnetic fields are reduced to values $\leq 2\mu$T by compensation coils located outside the vacuum apparatus. The electron energy resolution is limited by the bandwidth of the ionizing laser ($\Delta E_L \approx 0.15$ meV), residual electric fields ($\Delta E_F \leq 0.3$ meV), the Doppler effect, present in both the photoionization and in the attachment process (overall Doppler width $\Delta E_D \approx 0.1\sqrt{E}$ for 12.5% SF_6 seeded in He at $T_0 = 300$ K, ΔE_D and E in meV), and space charge broadening ΔE_{SC} due to K^+ photoions generated in the reaction volume ($\Delta E_{SC} \approx 0.6$ meV at 20 pA photocurrent, see Fig. 7 in [39]).

For the sake of in situ resolution testing and compensation of residual dc electric fields, test measurements of SF_6^- formation were frequently carried out, using a seeded supersonic beam of about 0.05% SF_6 in He ($p_0 = 1$ bar, $T_0 = 300$ K). As also addressed elsewhere in some detail [39], field compensation along the potassium beam direction is especially important in order to reduce the energy spread associated with the rise of the photoion-induced space charge potential and thus achieve optimum resolution. While the compensation potentials on opposite plates of the reaction chamber are typically small in the direction of the supersonic and laser beams (voltage in the range 0–30 mV), a much higher potential difference U_C (around 175 mV, see Fig. 2) is needed along the potassium beam direction (+ sign at upper entrance plate) for optimum performance. As discussed in detail in [5,7,34,40], residual electric fields lead to deformations of the measured anion yield from the true shape. For molecules such as SF_6 (s-wave attachment, cross-section $\sigma(E) \propto E^{-1/2}$ near zero energy) electric fields basically reduce the anion yield at very low electron energies. This loss is demonstrated in Figure 2 by plotting normalized ratios between the SF_6^- signals obtained at different compensation voltages U_C and the analytical cross-section $\sigma_{FIT}(E)$

$$\sigma_{FIT}(E) = (\sigma_0/E)[1 - \exp(-\beta E^{1/2})]. \qquad (3)$$

The cross-section (3) provides a very good overall description — at energies below 90 meV — of the experimental SF_6^- yield measured for a diffuse target gas at $T_G = 300$ K with sub-meV resolution [5,7,34,40] (i.e. with the choice $\beta = 0.405$ (meV)$^{-1/2}$ the smoothed original data points of the measurements deviate from the analytical fit (3) by no more than ±5%).

Figure 2 clearly demonstrates the electric field-induced deviations from the true cross-section behaviour. As expected the deviations are more or less the same for positive or negative detuning of the compensation voltage from the optimum setting. Electron optical simulations indicate that a compensation voltage U_C leads to a local compensation field F_C in the reaction center of $F_C \approx 10U_C$ [V m^{-1}]. With an uncertainty $\delta U_C \approx 0.02$ V for the optimum setting of U_C the residual dc electric field in the considered direction is compensated to values around 0.2 V m^{-1}. For the conditions of the present experiment the combined effects of residual and space charge-induced electric fields amount to an effective energy spread of ≤ 1 meV. Towards higher electron energies, the total energy spread will rise due to the increasing influence of the Doppler effect and reach about 2 meV at energies of 200 meV.

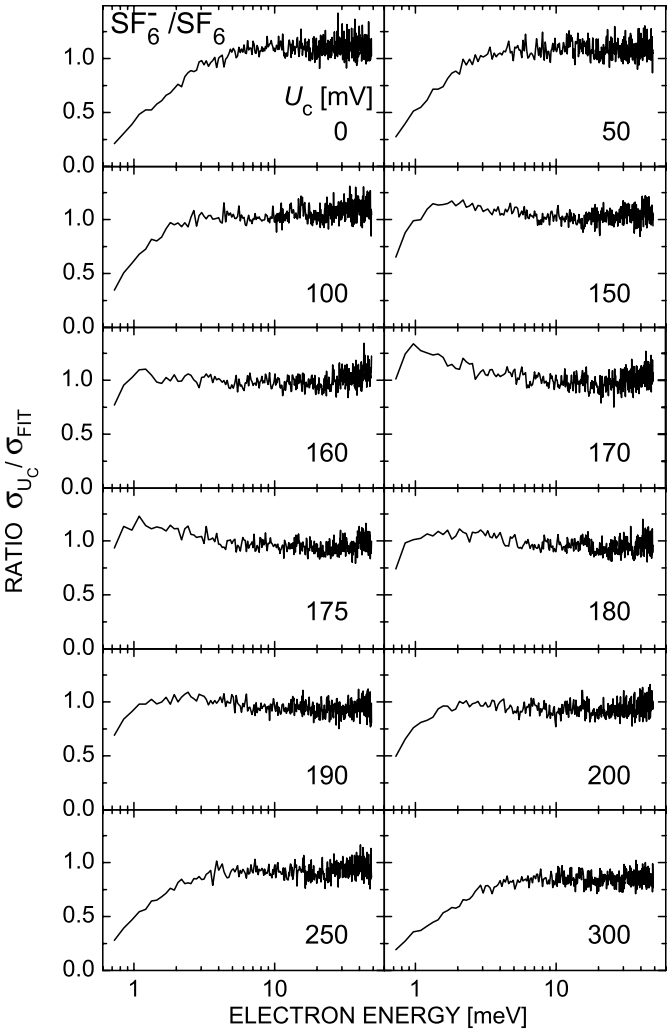

Fig. 2. Normalized ratios of measured SF_6^- yield and the cross-section (3) for compensation voltages U_C along the potassium beam direction ranging from 0 to 300 mV. Deviations of the ratios from unity at low electron energies are attributed to the presence of residual electric fields.

The use of a seeded supersonic beam target has the substantial advantage of a spatially confined reaction volume. Moreover, the light carrier gas helium leads to a substantial increase in the velocity of the SF_6 molecules (209 m s^{-1} for an effusive beam at 300 K). This has the disadvantage of an increased Doppler broadening. On the other hand, it results in an improved detection efficiency

of the product anions under conditions of weak or zero extraction field for which only those anions can be detected which are directed into the acceptance cone of the ion optics (laboratory half angle from the reaction center about 6°). In a mixed supersonic beam, containing the seeded minority component with molecular mass m_S at a fraction x and the atomic carrier gas with mass m_C (fraction $1-x$), the flow velocity u_S of the seeded component can be estimated (in the absence of velocity slip) by [41]

$$u_S \approx \{5k_BT_0/[xm_S + (1-x)m_C]\}^{1/2} \qquad (4)$$

with k_B = Boltzmann constant. For a seeded beam containing SF_6 at fractions $x = 0.0005/0.125$ in helium and expanding at $T_0 = 300$ K, one obtains $u_S(SF_6) \approx 1750/757$ m s^{-1}, respectively, i.e. SF_6 kinetic energies of 2.32 eV/0.43 eV. (We note that deviations from the velocities (4) due to velocity slip are expected to be below 10% [42]). At these energies, SF_6^- anions should be sampled very efficiently even in the absence of electric extraction fields in the reaction region. For DEA product ions such as SF_5^-, transverse velocity components attained in the dissociation process will in general lead to a reduction of the ions which enter the ion optics and thus have a chance to be imaged into the mass spectrometer. This fraction can be estimated when the translational energy release W in the center-of-mass (CM) frame is known. Fenzlaff et al. have shown [18] by time-of-flight analysis of the DEA product ions from SF_6 that the translational excess energy is thermal or quasi-thermal with a mean value below 0.15 eV. Assuming, for example, $W = 0.1$ eV for SF_5^- formation, the CM kinetic energy and velocity of the SF_5^- anions amount to 0.013 eV and 140 m/s, respectively. For isotropic dissociation of the temporary anion in the CM frame and at SF_6^- velocities of 1750 m/s and 757 m/s, the probability for SF_5^- ions to be emitted into the acceptance cone of the ion optics (half angle from the reaction center about 6°) amounts to 1 and to about 0.16, respectively (as compared to 1 for SF_6^-). Based on this estimate the SF_5^-/SF_6^- intensity ratio obtained with the 0.05% mixture is expected to exceed that measured with the 12.5% mixture at sufficiently low stagnation pressures (to prevent the effects of molecular cooling) by a factor of about 6. Measurements of the SF_5^-/SF_6^- intensity ratios obtained for the two mixtures at the same stagnation pressure $p_0 = 1$ bar for several nozzle temperatures (300–600 K) and electron energies below 0.2 eV (see Sect. 3.1) indicate that the kinetic energy release for SF_5^- formation may be even lower than 0.1 eV.

Another (nontrivial) aspect of DEA experiments is a possible influence on the anion detection probability associated with the angular distribution of the dissociating anions with respect to the momentum vector of the electron [43]. For electron beam experiments, this aspect may lead to different detection efficiencies of anions resulting from resonances with different symmetries, as long as anions are detected in an angle-sensitive manner. In the LPA experiment angular distribution effects are expected to be negligible (or small) because the photoelectrons, created in the center of the reaction region, are emitted in all directions (albeit not fully isotropically [37]).

2.2 Modified LPA experiment with extended energy range (EXLPA)

The standard LPA experiment, involving a variation of the electron energy by wavelength-tunable photoionization of laser-excited $K^*(4p_{3/2})$ atoms with a stilbene 3 dye laser, is limited to photoelectron energies up to about 200 meV. In order to extend the electron energy range we use a modified LPA method, denoted as EXLPA (EXtended Laser Photoelectron Attachment). In this approach, essentially zero energy photoelectrons are created in a separate photoionization chamber (designated PC, see Fig. 1), accelerated to variable energies and magnetically guided to the electrically field-free attachment region of the collimated, differentially-pumped supersonic target beam in the reaction chamber RC. Like RC, the photoionization chamber PC consists of six plates to which independent potentials can be applied. RC and PC are separated by three plates with circular apertures of 3 mm diameter. The respectively adjacent plates are electrically connected to RC and PC while the intermediate plate has an independently variable potential. Under typical operating conditions, photoelectrons are created in PC very close to threshold (nominal kinetic energy below 0.2 meV) and extracted with a voltage $U_{EX} \approx 0.6$ V (extraction field about $F_{EX} \approx 15$ V m^{-1}). To reduce the energy spread associated with the potential drop across the photoionization region the ionizing intracavity dye laser is focussed into the photoionization region with antireflection-coated spherical lenses. Ray tracing calculations yield a diameter of the ionizing laser in the region of overlap with the potassium beam of about 0.12 mm. With $F_{EX} \approx 15$ V m^{-1} one thus expects an energy spread of about 2 meV.

While magnetic fields are carefully reduced to values ≤ 20 μT in the standard LPA method, a nearly homogeneous magnetic field of about 0.002 T (produced by two current coils in near-Helmholtz configuration outside the vacuum chamber) is applied in the modified LPA approach along the potassium beam direction. This field guides the electrons towards the reaction volume with the supersonic target beam and further through the entrance aperture (3 mm diameter) of the electron collector. For a proper operation of the experiment, extreme care has to be taken to avoid any collisions of the electron beam with surfaces on its way from the photoionization chamber to the collector since these would yield spurious low-energy electrons and thus lead to unwanted attachment processes, especially critical in energy ranges where the attachment cross-section is small. This requires a careful alignment of the focus position of the ionization laser in PC. For this purpose, the two spherical lenses can be moved with precision translational mounts in both directions orthogonal to the laser direction. With optimal laser alignment an effective energy width of 20 meV was achieved and the drop of the SF_6^- cross-section towards higher electron energies could be followed over five orders of magnitude (see Sect. 3.3).

3 Results and discussion

3.1 Diagnostics of the molecular temperature

One of the important aspects of the present study is the variation of the energy-dependent yield for the different product anions with the internal energy of the molecule. In a seeded supersonic beam the internal molecular temperature T_i is not simply given by the nozzle temperature T_0 since cooling of the rotational and vibrational degrees of freedom occurs in a way which depends on stagnation pressure p_0 and nozzle diameter ($d_0 = 60$ μm fixed). For the gas mixtures used in the present work it is likely that the rotational degree of freedom will be efficiently cooled while cooling of the vibrational degrees of freedom occurs less rapidly. Since we did not have access to a direct method of analyzing the rovibrational temperature of the SF_6 molecules (e.g. by IR excitation) we tried to obtain some information on the internal temperature T_i by measuring the anion ratio $R \equiv Y(SF_5^-)/Y(SF_6^-)$ of the yields for SF_5^- and SF_6^- formation for four nozzle temperatures (300, 400, 500, and 600 K) and three stagnation pressures (1, 2, 3 bar) at several electron energies (10, 90, 180 meV). It is well known that the yield for SF_5^- anions at near-zero electron energies from a thermal ensemble of SF_6 molecules grows strongly with rising gas temperature [2,12,16,44–47]. Thus the idea is to use the ratio R as a molecular thermometer.

Before we describe our results, we briefly survey previous findings. Using flowing afterglows, the temperature dependence of the ratio R has been investigated by Fehsenfeld [44] and by Miller et al. [45] under conditions of equal gas and electron temperatures. Close to 300 K, anion ratios of 0.6×10^{-4} [44] and 7.2×10^{-4} [45] have been reported. At higher temperatures (e.g. 477 K), much higher ratios (about 4% [44] and 8% [45]) were observed, and these authors consistently reported activation energies for SF_5^- formation of 0.43 eV [44] and 0.42 eV [45]. Electron beam work of Kline et al. [13] yielded $R \approx 0.64\%$ (taken from Fig. 3 in [13]) at near-zero electron energy and room temperature. Chen and Chantry [12] (who quote a value of 4% at near-zero electron energy and a gas temperature of $T_G = 390$ K) reported an increase of R by a factor of about 230 when the gas temperature was raised from 300 K to 880 K (Fig. 1 in [12]); from this dependence they extracted an activation energy for SF_5^- formation of 0.20 eV. Our findings are summarized in Figure 3.

The results with the dilute gas mixture (0.05% SF_6 in He, denoted by stars) exhibit a strong exponential increase of the ratio R with rising nozzle temperature. We note that these values (especially the slope) are close to those found earlier in our group [48] with an effusive, differentially pumped beam of pure SF_6 (using a set-up described in our work on RET to C_{60} and C_{70} [49]); this agreement suggests that (vibrational) cooling is weak for SF_6 molecules in the dilute gas mixture. The ratios agree — at least qualitatively — with those found in the afterglow experiments [44,45] and in the electron beam study [12].

The ratios R measured for the 12.5% mixture lie below those for the 0.05% mixture (except at $T_0 = 300$ K, see below), but a direct comparison between the results for the two gas mixtures is hampered by the fact that the detection efficiency for the SF_5^- ions may be different in the two cases (see Sect. 2.1). At the two highest temperatures (for which the clearest results are obtained) the ratios R with the dilute mixture exceed those for the 12.5% mixture at the same stagnation pressure (1 bar) by factors of 2–2.5 (see Fig. 3). If the kinetic energy release for SF_5^- formation were zero (yielding the same SF_5^- detection efficiency with the two gas mixtures) these differences could be attributed to a reduction in molecular temperature by 30–50 K in going from the dilute to the 12.5% mixture. On the other hand — assuming that molecular cooling can be neglected for both gas mixtures at $p_0 = 1$ bar — this difference could be attributed to a reduced SF_5^- detection efficiency in the case of the 12.5% mixture. At $T_0 = 600$ K an assumed kinetic energy release of $W = 0.1$ eV is

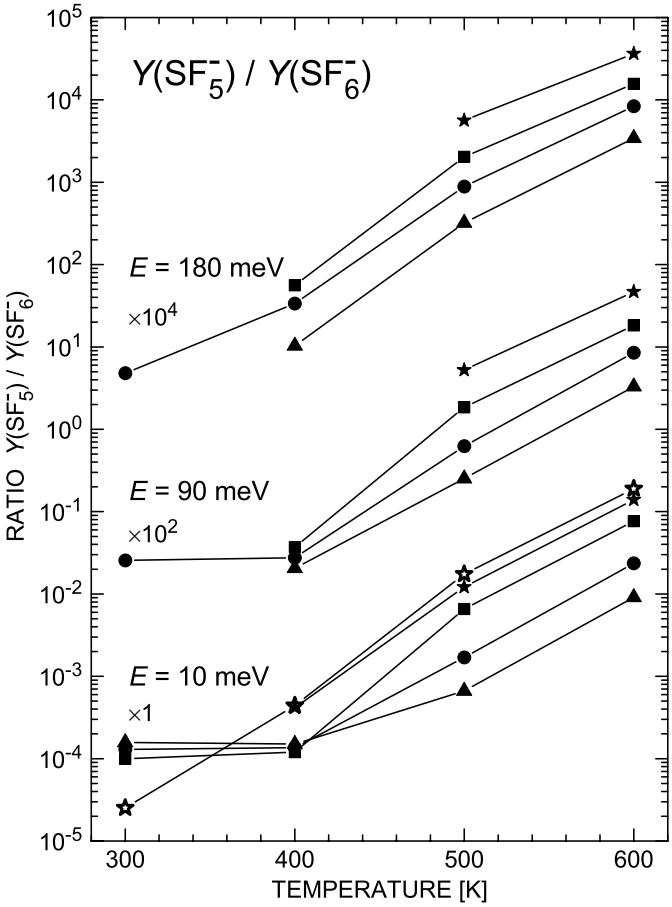

Fig. 3. Ratio $R = Y(SF_5^-)/Y(SF_6^-)$, as obtained for a seeded supersonic beam of 12.5% SF_6 in He at the stagnation pressures $p_0 = 1$ bar (full squares), 2 bar (full circles) and 3 bar (full triangles) and four nozzle temperatures T_0 for the three electron energies 10 meV (lower panel), 90 meV (middle) and 180 meV (upper panel). In the lower panel we have included results obtained with a mixture of 0.05% SF_6 in He at $p_0 = 1$ bar (full stars); the ratios shown by open stars were obtained with the same mixture, but using Rydberg electron transfer (RET) at very high principal quantum numbers ($n \approx 250$).

estimated to cause a reduction by a factor of 3.3, somewhat higher than the observed difference. We conclude that the kinetic energy release for SF_5^- formation is below 0.1 eV at electron energies below 0.2 eV and temperatures $\leq$ 600 K. Moreover, we conclude that the internal temperature T_i of the SF_6 molecules in the seeded supersonic beam (12.5% SF_6 in He) at $p_0 = 1$ bar and higher nozzle temperatures is lower than that for the SF_6 molecules in the dilute mixture by no more than about 50 K.

The clearest information on the internal temperature of the SF_6 molecules in the seeded supersonic beam was obtained by comparing the shapes of the higher energy peak in the SF_5^- attachment spectra (see Sect. 3.4, in particular Fig. 7), measured at different nozzle temperatures and stagnation pressures, with the shape obtained very recently for SF_6 molecules at $T_i = 300$ K (using a modified EXLPA method, involving pulsed electron production and ion extraction and a static, thermal SF_6 target at room temperature [50]). The shape of the higher energy peak for SF_5^- formation in the $T_i = 300$ K data agrees closely with that observed in the present work for a nozzle temperature of $T_0 = 400$ K at $p_0 = 1$ bar (see Fig. 7). In the thermal data, the peak maximum is located at about 0.55 eV and the SF_5^- yield in the minimum (located at about 0.13 eV) amounts to about 12% of the maximum at 0.55 eV [50]. It thus appears that for the seeded supersonic beam (12.5% SF_6 in He) at $T_0 = 400$ K and $p_0 = 1$ bar the internal SF_6 temperature is about 100 K lower than the nozzle temperature. In conjunction with the results in Figure 3 (which suggest that at $T_0 = 400$ K the SF_6 molecules in the 12.5% mixture are about 50 K colder than in the dilute mixture) we have to conclude that the molecules in the dilute mixture have been cooled to a (vibrational) temperature about 50 K below the nozzle temperature. As a simple guide we can use the relation $T_i = T_0 - 100$ K for the 12.5% mixture expanded at $p_0 = 1$ bar.

With rising stagnation pressure (as clearly signaled by the data taken at 500 K and 600 K) the molecular temperature is significantly reduced. A rise from 1 bar to 3 bar leads to a reduction in temperature by about 100 K. The ratios measured for the 12.5% mixture at $T_0 = 300$ K (both at 10 meV and 90 meV) do not follow the general trend and appear to be too high. We offer two tentative explanations for these observations. (i) Although cluster formation is rather weak for SF_6 (see e.g. the RET results in [51]) it cannot be ruled out that at the lower temperatures (most notably at 300 K) SF_5^- formation may contain weak contributions due to electron capture by SF_6 clusters with subsequent dissociation/evaporation; we cannot quantify, however, such contributions. (ii) Another possibility is collision-induced dissociation (CID) of a small fraction of the primary SF_6^- anions yielding SF_5^- which are subsequently detected. According to studies of Ferguson et al. (Fig. 9 in [52]) and Wang et al. [53] the cross-section for SF_5^- formation in collisions of SF_6^- ions with SF_6 molecules rises strongly with relative kinetic energy E_{rel} and reaches values of (10–20)$\times 10^{-20}$ m^2 at collision energies from 2–50 eV. (The cross-section for collisional electron detachment in SF_6^- + SF_6 collisions stays below 10^{-20} m^2 at relative kinetic energies below 100 eV, (Fig. 10 in [53]). Cross-sections for SF_5^- formation due to CID in SF_6^- + He collisions are around 14×10^{-20} m^2 for collision energies of 3–10 eV [53]. In the present experiment CID of the accelerated SF_6^- ions, colliding with SF_6 molecules or with He atoms in the seeded supersonic beam, may occur in the ion optics and in the mass spectrometer with relative kinetic energies of up to about $E_{rel} = 5$ eV (for SF_6^- + SF_6) and of up to $E_{rel} = 0.15$ eV (for SF_6^-+He). It is likely that CID in SF_6^- + He collisions is not yet efficient at relative kinetic energies as low as 0.15 eV, and we thus discard these collisions as a source for SF_5^- ions. Assuming an effective path length for CID of 2 cm and an (estimated) SF_6 density of 5×10^{10} cm^{-3} in the relevant region for the 12.5% mixture at stagnation pressures ≥ 1 bar, a fraction around 10^{-4} of the primary SF_6^- ions may be converted to SF_5^- ions via CID in SF_6^- + SF_6 collisions. Thus CID in this collision system may in fact contribute to the SF_5^- signal observed at $T_0 = 300$ K and *low* electron energies, but we are not able to quantify this possible CID contribution (see also the discussion in Sect. 3.5).

Independent information on possible CID contributions to the SF_5^- signal at near-zero electron energy comes from a recent EXLPA study of anion formation from a diffuse SF_6 target at $T_i = 300$ K [50]: when the target density in the reaction chamber was raised by a factor of almost 6 from about 1.4×10^{10} cm^{-3} to 8×10^{10} cm^{-3} the ratio $R = Y(SF_5^-)/Y(SF_6^-)$ (measured at near-zero electron energy) increased by a factor of 1.6, pointing to a possible CID contribution of no more than 40% at the higher density.

It should be emphasized that the intensity ratios R reported here and in previous work are subject to uncertainties associated with the (possibly different) detection efficiencies of the two ion species SF_6^- and SF_5^-. These efficiencies are influenced by several factors: (i) ion extraction and imaging efficiency reflecting the probability that a formed anion is injected into the mass spectrometer; (ii) anion transmission of the mass spectrometer; (iii) anion detection efficiency at the channel electron multiplier. It is likely that the efficiencies (ii) and (iii) are (nearly) identical for SF_6^- and SF_5^- in view of their similar masses. In the present set-up involving a collimated target beam and geometrical sampling (no extraction field) of the anions the efficiencies (i) may be lower for the SF_5^- ions in a way which depends on the velocity of the SF_6 molecules and on the center-of-mass kinetic energy release for the SF_5^- ions, as discussed above. From this point of view, the anion ratios $R = Y(SF_5^-)/Y(SF_6^-)$ in this paper have to be regarded as lower limits.

3.2 On the possible influence of SF_6^- autodetachment

There is yet another aspect of the anion detection efficiency which pertains specifically to the detection of *metastable* anions such as SF_6^-, namely their lifetime τ towards autodetachment (which depends on the primary internal energy and on the electron energy) in comparison

with the time span (here denoted as detection time t_D) from the formation to the detection of these anions. Controversial results have been reported for the autodetachment lifetimes of SF_6^- anions. Experiments with time-of-flight (TOF) mass spectrometers [19,20,22,27,28,32] yielded SF_6^- lifetimes below 100 μs. In contrast much longer lifetimes (up to several ms) were observed in experiments using ion-cyclotron-resonance (ICR) mass spectrometry [21,23,24]. In the most recent TOF work of Le Garrec et al. [32] SF_6^- ions were created by attachment of photoelectrons produced by laser photoionization of Na atoms (initial photoelectron energies 0–100 meV); the SF_6 target was produced by supersonic expansion of pure SF_6 ($T_0 = 300$ K) with a pulsed valve (resulting in rovibrational cooling of the SF_6 molecules). From their data the authors extracted a lifetime for loss of the SF_6^- ions (attributed to autodetachment) of 19.1(27) μs. This result is in strong contrast with the findings of the Rice group [30,31,33] who studied the autodetachment stability of SF_6^- created in RET from state-selected, laser-excited $K^{**}(np)$ Rydberg atoms ($n = 30$–60) to thermal SF_6 molecules ($T_i = 300$ K). Using TOF techniques (flight times in the 5–35 μs range) [30,31] as well as magnetic traps for exploring the evolution over longer times up to about 10 ms [33], they found no evidence for the presence of SF_6^- ions with 'short' lifetimes (below 100 μs). Their TOF data [31] suggest a lower limit for the lifetime of about 300 μs. Their magnetic trap work yielded a lifetime against autodetachment of several ms [33], compatible with the value reported earlier for SF_6^- ions formed in $Xe^{**}(31f)$+SF_6 collisions [29]. One might argue that the RET process produces SF_6^- with longer lifetimes as a result of stabilizing energy exchange in postattachment collisions between the positive ion and the SF_6^- anion. This argument becomes relevant at low principal quantum numbers while at, e.g. $n = 60$ the fraction of Coulombic complexes which may undergo stabilizing collisions is only about 5% [33]. Even at $n = 30$ this fraction is no larger than 25% [33]. Thus, the discrepancy between the TOF results of Le Garrec et al. [32] and those of the Rice group [30,31,33] is a real puzzle.

In the present set-up, we estimate the ion detection time for SF_6^- anions to be about 97 μs and 115 μs for the 0.05% and 12.5% target gas mixture, respectively ($T_0 = 300$ K). For RET at high n, we thus expect negligible SF_6^- losses due to autodetachment, assuming lifetimes of the SF_6^- anions in the ms range [33] due to autodetachment at $T_0 = 300$ K. Comparing the RET-induced SF_6^- signals with those due to free electron attachment at low energies on the basis of the known rate coefficients for the two processes [5,6,54] we conclude that the autodetachment lifetimes of the SF_6^- anions due to free electron attachment must be longer than our anion detection time (i.e. at least about 300 μs and possibly as long as those of the SF_6^- anions due to RET). Thus, the lifetime of 19.1(27) μs reported by Le Garrec et al. [32] for low-energy free electron attachment appears questionable. A speculative, counter-intuitive physical cause for the short lifetime reported in [32], connected with a low internal temperature of the SF_6 molecules (as expected for the experiment in [32]), might be that longer autodetachment lifetimes are bound to the presence of some minimum initial vibrational excitation to facilitate the scrambling of vibrational energy in the SF_6^- complex which is needed to prevent fast autodetachment. On the other hand, other TOF experiments [19,20] involving SF_6 molecules at $T_i \approx 300$ K also yielded SF_6^- lifetimes similar to that of Le Garrec et al. [32], suggesting that this speculative cause does not apply.

In order to establish relative anion yields for different nozzle temperatures at fixed stagnation pressure, the measured anion intensities have to be corrected for variations in the molecular target density and in the respective anion detection efficiencies. Measurements of positive ion mass spectra (SF_5^+ signal) qualitatively indicated that — as expected — the target density followed a T_0^{-1} behaviour (note that the gas flow into the nozzle chamber follows, as found experimentally, a $T_0^{-1/2}$ dependence at fixed stagnation pressure and thus the target density should obey a T_0^{-1} dependence since the flow velocity increases as $T_0^{1/2}$ with rising T_0). EXLPA measurements of the energy-integrated SF_6^- signals and of the zero-energy peak intensities at the fixed stagnation pressure $p_0 = 1$ bar (12.5% SF_6 in He) as a function of nozzle temperature ($T_0 = 300$–600 K) yielded density-corrected anion yields (i.e. signals multiplied by T_0) which at each temperature coincided to within 15% or less and which varied by no more than ±20% over the range 300–600 K. We consider this as our uncertainty for our relative anion yields for SF_6^- formation at different temperatures. Previous electron beam [55] and swarm studies [1,2,44,45,56,57] indicate that the attachment rate coefficient for SF_6 is essentially constant over the temperature range of interest (we note that experiments of Le Garrec et al. [58] yielded lower values at temperatures between 48 and 170 K); we thus conclude that the SF_6^- anion intensities are only weakly (if at all) influenced by autodetachment losses at *low* electron energies and nozzle temperatures of 300–600 K.

3.3 Attachment spectra for SF_6^- formation

In Figure 4 we present attachment spectra for SF_6^- formation over the electron energy range 1–200 meV, as obtained with SF_6 molecules having an internal temperature close to 300 K. For a clearer display of structure it is helpful to compensate for the $E^{-1/2}$ decrease of the cross-section associated with s-wave behaviour of the attachment process; thus we have chosen to plot the energy dependent rate coefficients $k_A(E) = (2E/m)^{1/2}\sigma_A(E)$ (m = electron mass) which converge to a constant value at very low electron energies E. For clarity the different neighbouring data sets have been displaced by factors of two as indicated in Figure 4. The upper full curve (a) represents the result of a recent calculation of SF_6^- formation, carried out in the framework of Effective Range Theory (ERT) [59]. In an attempt to analyze the available experimental low-energy electron collision data on SF_6,

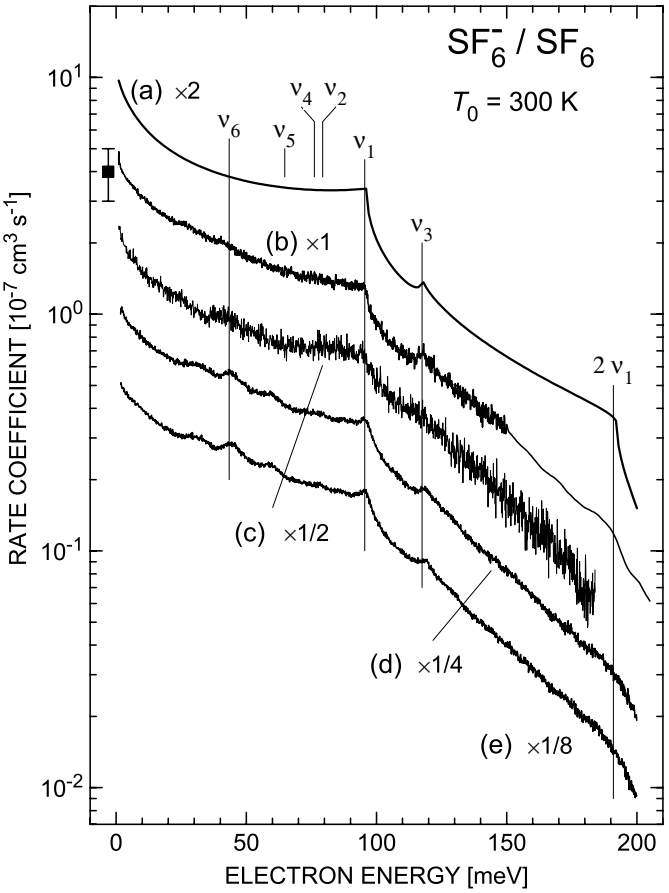

Fig. 4. Energy-dependent rate coefficients for SF_6^- formation with near thermal (300 K) SF_6 target molecules. (a) ERT calculation [59], see text. (b) LPA experiment [5,40]. (c) Supersonic target beam with 0.05% SF_6 in He, $p_0 = 1$ bar, $T_0 = 300$ K. (d) Supersonic target beam with 12.5% SF_6 in He, $p_0 = 1$ bar, $T_0 = 300$ K. (e) Supersonic target beam with 12.5% SF_6 in He, $p_0 = 2$ bar, $T_0 = 300$ K. Full square with error bar: RET rate coefficient at high principal quantum numbers [6]. For clarity, the different data traces have been displaced by the indicated factors.

Fabrikant et al. [59] adjusted the parameters of their ERT model to the low-energy behaviour of the total scattering cross-section due to Field et al. [60] and to the absolute attachment cross-section of Klar et al. [5,40], both measured at the gas temperature 300 K. The data set (b) shows the LPA rate coefficients, reported in [5] for a diffuse SF_6 target gas at $T_G = 300$ K over the range 0.2–170 meV and extended by Schramm et al. [40,48] to higher energies in an experiment with a skimmed supersonic beam of pure SF_6 ($T_0 = 300$ K; $p_0 = 1$ bar). The anion rates (c), (d), and (e) were measured in the present work with the supersonic beam target for the fixed nozzle temperature $T_0 = 300$ K at a stagnation pressure of $p_0 = 1$ bar for 0.05% SF_6 in He (c) and for 12.5% SF_6 in He (d) while the data (e) were obtained at $p_0 = 2$ bar for the 12.5% mixture. The rate coefficient for the data set (b) has been normalized to the thermal attachment rate coefficient $k_A(T_G = T_e = 300\ \mathrm{K}) = 2.27(9) \times 10^{-7}$ cm^3/s [44,45,57] and the rates (c), (d), and (e) have been adjusted to the rate of (b) at the lowest energies. In good agreement with the ERT calculation, all experimental spectra are characterized by a more or less monotonical decrease with rising energy and a prominent downward cusp structure at the onset for vibrational excitation of the symmetric stretch mode ($\nu_1 = 1$, A_{1g} symmetry) [2] close to 96 meV as well as weak peak structure at the $\nu_3 = 1$ vibrational onset (117.5 meV, degenerate stretch, F_{1u} symmetry) [2] due to interaction between the attachment and the vibrational excitation channels. The spectra also show a downward cusp at the $\nu_1 = 2$ onset near 190 meV. We note that the main features of this behaviour were already recovered in an earlier zero-range theory description of low-energy electron attachment to SF_6 by Gauyacq and Herzenberg [61]. The rate coefficient at energies very close to zero ties in nicely with the independently determined rate coefficient for Rydberg electron attachment to SF_6 at high principal quantum numbers $k_{nl} = (4 \pm 1) \times 10^{-7}$ cm^3/s [6,62], as discussed before [5,6,54].

The agreement between the four experimental data sets shown in Figure 4 has to be considered as very good in view of the fact that they were obtained with different methods and targets. The agreement actually supports the conclusion drawn in Section 3.1 that the internal temperature T_i of the SF_6 molecules in the dilute (0.05%) and in the 12.5% mixture expanded at 1 bar at $T_0 = 300$ K is rather close to 300 K. The close agreement between the rates (d) and (e) demonstrates that at $T_0 = 300$ K the rise of the stagnation pressure from 1 bar to 2 bar has (almost) no effect on the SF_6^- attachment spectrum at electron energies below 200 meV.

Compared to the spectra (b) and (c), the data (d) and (e) show some additional peak structure at energies of 32, 44, and 59 meV. The clearest peak at 44 meV (corresponding to a local increase of about 25%) can be associated with the onset for the $\nu_6 = 1$ vibrational channel (degenerate deformation, F_{2u} symmetry) [2] while the origin of the other two features is not obvious; they do not seem to be connected with onsets for other vibrational modes [2] (see thresholds indicated in Fig. 4). We note that peak structure around 46 meV has been recently reported by Howe et al. [8] in a high resolution electron attachment experiment involving a pulsed supersonic target beam (10% SF_6 seeded in Xe, $T_0 = 300$ K). An improved variant of the TPSA method [4] was used by photoionizing Xe atoms above the $Xe^+(^2P_{1/2})$ threshold with coherent narrowband VUV radiation of sub-meV width [8]. Apart from the peak at 46 meV, Howe et al. also found clear (peak) structure at the $\nu_1 = 1$ and the $\nu_3 = 1$ vibrational onsets. The general decrease of their cross-section in the range 0–90 meV was less pronounced than in the LPA cross-section [5], suggesting values of β in the range 0–0.228 meV$^{-1/2}$ (the latter being the Klots prediction $\beta\ E^{1/2} = (2\alpha E)^{1/2}$ [9,63] for electron capture by a non-dipolar molecule with a polarizability α identical to that of SF_6 ($\alpha = 44\ a_0^3$ [2], a_0 = Bohr radius). We attribute the additional peak structure in the attachment spectra of Howe et al. [8] and in our data with the 12.5% mixture to

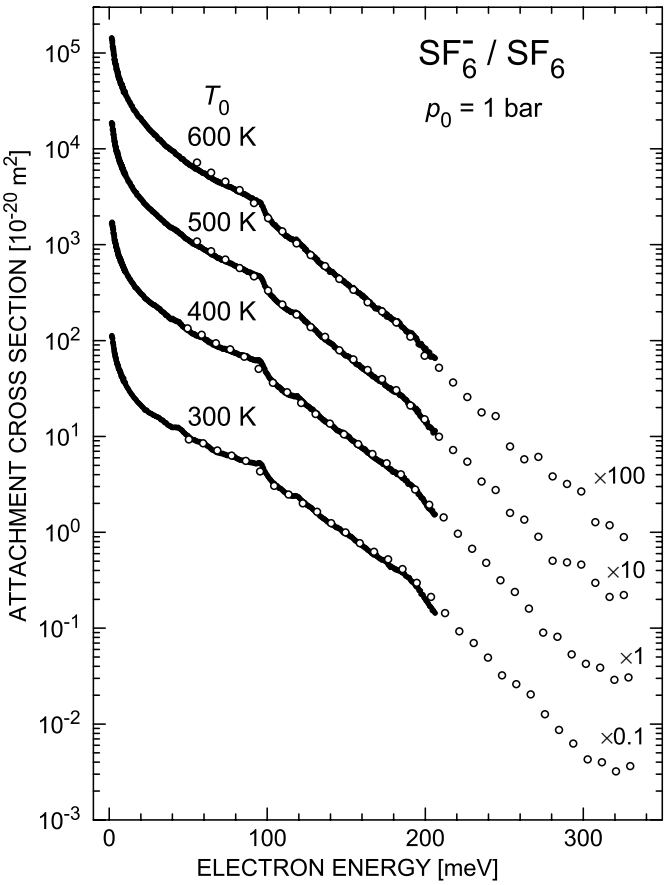

Fig. 5. Cross-sections for SF_6^- formation (combined LPA (full symbols) and EXLPA data (open symbols)) measured with the supersonic beam target (12.5% SF_6 in He) at $p_0 = 1$ bar at the four nozzle temperatures $T_0 = 300$, 400, 500, 600 K. For clarity, the data for the neighbouring temperatures have been displaced by factors of 10 or 1/10, respectively.

the effects of molecular cooling and/or clustering (i.e. SF_6^- formation due to attachment to $(SF_6)_N$ $(N \geq 2)$ clusters followed by evaporation of $(N-1)$ SF_6 molecules). As will be documented by the data presented in Figure 5 the additional structure disappears at higher temperatures.

In Figure 5 we present cross-sections for SF_6^- formation, measured with the supersonic beam target (12.5% SF_6 in He) at $p_0 = 1$ bar for the four nozzle temperatures $T_0 = 300$, 400, 500, and 600 K. The results represent the combined LPA and EXLPA data of the present work. The LPA and EXLPA anion yields (obtained from the measured anion signals after correction for the temperature dependent density, see above) were normalized to each other at energies above 50 meV where the effects of the poorer resolution in the EXLPA data are negligible (except for the reduced clarity of vibrational structure). The LPA and EXLPA anion yields agree well in the energy range 50–200 meV at all four temperatures. The absolute cross-section scale in Figure 5 has been fixed by normalizing the anion yield for $T_0 = 400$ K (which corresponds to a molecular temperature close to 300 K, see Sects. 3.1 and 3.4) with reference to the energy-dependent rate coefficients at $T_i = 300$ K [5] shown in Figure 4. The absolute cross-sections at the other temperatures T_0 are expected to have an additional uncertainty of about ±30%.

The overall energy dependence shows only weak variations with nozzle and thus internal temperature. The additional structure in the energy range 30–90 meV progressively disappears with rising temperature. Above 200 meV the cross-section falls exponentially by a factor of 40–50 per 100 meV energy increase. The overall decrease of the anion yield towards higher electron energies gets larger with rising temperature; over the range 1–300 meV the decrease amounts to a factor of 3×10^4 and 10^5 at the nozzle temperatures 300 and 600 K, respectively. Possibly, this different behaviour is (at least in part) related to the effects of autodetachment. In order to discuss this variation we assume that the observed effective cross-section for SF_6^- formation can be written as

$$\sigma(E;T_0) = \sigma_c(E) p_{AD}(E;T_0) \tag{5}$$

where $\sigma_c(E)$ denotes the primary electron capture cross-section which is assumed to be independent of the internal temperature and thus of T_0. (We note that a weak dependence of the capture cross-section on the initial symmetric stretch vibrational state ν_1 has been recently predicted [64], capture through the virtual state being more efficient from lower ν_1 levels.) The factor $p_{AD}(E;T_0)$ represents the influence of autodetachment on SF_6^- detection; it depends on the experimental anion detection time t_D and is given by $p_{AD}(E;T_0) = \exp[-t_D/\tau(E;T_0)]$. At low electron energies E and $T_0 = 300$ K the factor $p_{AD}(E;T_0)$ is close to unity in our experiment since the autodetachment lifetime is substantially longer than the anion detection time (see above). The data discussed in Section 3.2 indicate that $p_{AD}(E;T_0)$ is not much lower than unity even at $T_0 = 600$ K and *low* electron energies. The values of $p_{AD}(E;T_0)$ at higher electron energies, however, may be significantly lower than unity, even at 300 K.

The following information on $p_{AD}(E;T_0)$ may be obtained from the temperature dependence of the observed effective cross-sections at higher electron energies. For a particular electron energy the ratio of the cross-sections at two temperatures (say at 300 K and 600 K) is given by

$$\begin{aligned}\sigma(E;T_{0,1})/\sigma(E;T_{0,2}) &= \\ &\sigma_c(E)p_{AD}(E;T_{0,1})/[\sigma_c(E)p_{AD}(E;T_{0,2})] \\ &= \exp[-t_{D1}/\tau(E;T_{0,1})]/\exp[-t_{D2}/\tau(E;T_{0,2})].\end{aligned} \tag{6}$$

Note that the detection times depend somewhat on the nozzle temperature (decreasing from 115 μs to 106 μs for the 12.5% mixture when T_0 rises from 300 K to 600 K). At $E = 200$ meV, for example, the observed ratio $\sigma(E;300\text{ K})/\sigma(E;600\text{ K}) \approx 3$ leads to the relation $t_{D2}/\tau(600\text{ K}) = \ln 3 + t_{D1}/\tau(300\text{ K})$. For the case $t_{D1}/\tau(300\text{ K}) \ll 1$, one obtains $\tau(600\text{ K}) = t_{D2}/\ln 3 \approx 96$ μs. If $t_{D1}/\tau(300\text{ K}) = 1$ (which appears to be unlikely in view of the lower bound/$\tau(300\text{ K}) \geq 300$ μs, see above), one gets $\tau(600\text{ K}) = t_{D2}/(1+\ln 3) \approx 50$ μs. At $E = 300$ meV, the observed ratio $\sigma(E;300\text{ K})/\sigma(E;600\text{ K})$ is nearly the same as at $E = 200$ meV. To gain further

insight, a future direct measurement of the effective SF_6^- lifetime at well-defined higher electron energies and for different internal molecular temperatures would be of great interest and importance.

Some information may be drawn on possible effects of SF_6^- autodetachment at the higher electron energies for $T_i \approx 300$ K with reference to the recent calculation of SF_6^- formation, carried out in the framework of Effective Range Theory [59]. There is good overall agreement between the calculated rate and the experimental LPA rate (see Fig. 4). Some deviations are observed below the onsets for excitation of one and two quanta of the symmetric stretch mode ν_1 where the calculated rate stays above the measured rate by up to 30%, but there is no systematic trend that the experimental data progressively stay below the theoretical rate coefficients with rising electron energy. Such a trend could be interpreted to reflect losses in the experimental anion yield due to autodetachment. We conclude that there is no evidence from the spectra presented in Figure 4 that the lifetime of SF_6^- anions, formed from SF_6 molecules with internal temperatures of 300 K (or somewhat below) and at electron energies up to 200 meV, is similar to or shorter than the anion detection time (40–120 μs for the earlier [5,65] and about 115 μs in the present LPA experiment). We note that additional ERT calculations of the SF_6 attachment cross-sections with somewhat different parameter sets (but keeping agreement with the experimental data at low electron energies) [64] resulted in cross-sections which are *lower* than the ERT cross-sections shown in Figure 4, especially above the onset for $\nu_1 = 1$ excitation.

We conclude this sub-section by mentioning an interesting observation made at higher electron energies when the stagnation pressure p_0 was raised from 1 bar to 5 bar. Figure 6 shows the SF_6^- anion yield measured with the EXLPA method for $p_0 = 1$, 2, 3, and 5 bar at $T_0 = 300$ K.

Above about $E = 300$ meV the yield functions show a clear change in slope with a *much slower decrease* of the anion yield at higher electron energies. At higher nozzle temperatures, this effect was found to be much less pronounced. We envision two possible explanations for this behaviour. (i) Assuming that clusters can be ignored as possible precursors for the detected SF_6^- anions, the observation in Figure 6 may indicate the formation of sufficiently long-lived SF_6^- anions through an *additional* channel, i.e. via a different potential surface with an attachment threshold close to 300 meV. The observation of this channel requires sufficiently cold SF_6 molecules as present at higher stagnation pressures. (ii) As an alternative possibility, we suggest that the signals, progressively observed at energies above 300 meV, stem from SF_6 clusters which are formed with rising fractions towards higher stagnation pressures. During the present experiments we did not investigate the cluster anion mass spectra at higher electron energies and different stagnation pressures in detail nor did we try to measure the energy dependence of cluster anion yields. These would be interesting topics for future studies.

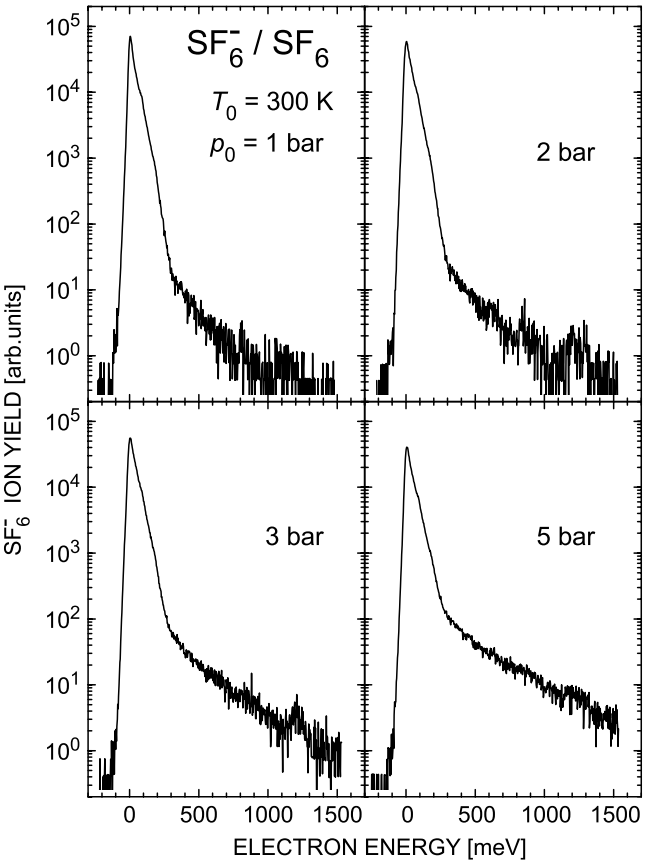

Fig. 6. Energy-dependent yield for SF_6^- formation measured with the EXLPA method at the fixed nozzle temperature $T_0 = 300$ K for the four different stagnation pressures $p_0 = 1$, 2, 3, 5 bar. Note the tail above 0.3 eV which rises with increasing pressure and decreases rather slowly with rising electron energy. Some structure in the spectra taken at $p_0 = 2$, 3, and 5 bar which appears at higher electron energies (near 0.8 eV and 1.2 eV) is due to contributions from electrons inelastically scattered from one of the orifices between PC and RC. These features are absent for optimal alignment. The shown anion yields reflect the measured signals without an attempt to correct for possible changes in target density.

3.4 Attachment spectra for SF_5^- formation

In Figure 7 we present anion yields for SF_5^- formation, obtained with the supersonic beam target (12.5% SF_6 in He) at $p_0 = 1$ bar for the four nozzle temperatures $T_0 = 300$, 400, 500, and 600 K over the energy range 1–1500 meV. The results represent the combined LPA and EXLPA anion yields (obtained from the measured signals after correction for the T_0-dependent target density), as normalized to each other at energies above 50 meV where the effects of the broader energy width in the EXLPA data are negligible. We note that the present LPA results (shown for $E \leq 185$ meV) represent the first SF_5^- attachment spectra measured at meV resolution.

The major observations documented in Figure 7 can be summarized as follows: the SF_5^- yield is composed of a sharp peak at near-zero energies whose intensity rises

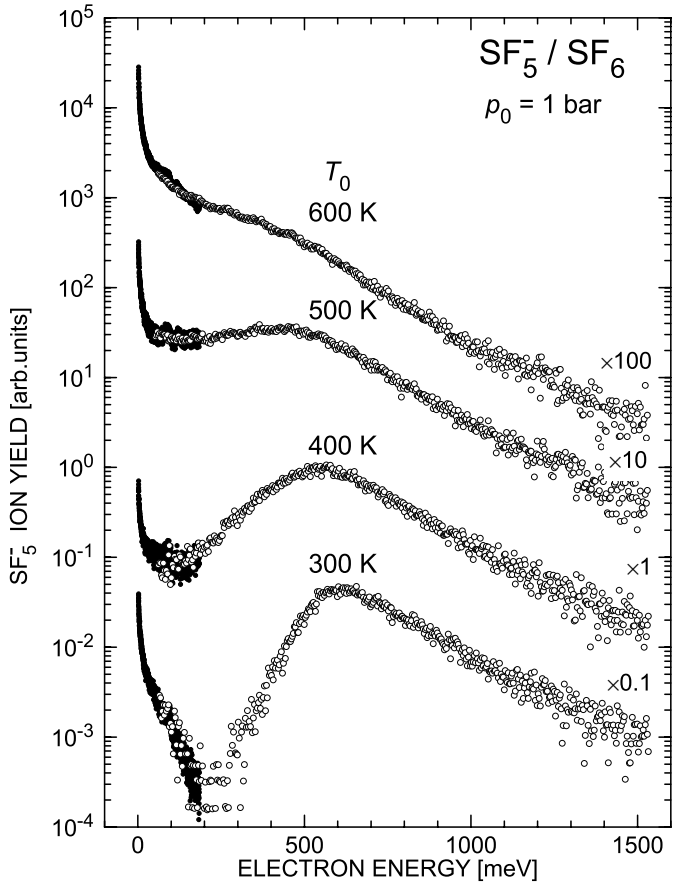

Fig. 7. Energy dependent yields for SF_5^- formation (combined LPA (full symbols) and EXLPA data (open symbols)) obtained with the supersonic beam target (12.5% SF_6 in He) at $p_0 = 1$ bar for the four nozzle temperatures $T_0 = 300$, 400, 500, 600 K. For clarity, the data have been displaced by factors of 10, respectively. The ordinate scale for the $T_0 = 400$ K data (when multiplied by 10^{-20} m^2) presents the absolute cross-section for SF_5^- formation which is found to agree with the recommended absolute cross-section for this process at energies above 1 eV [2].

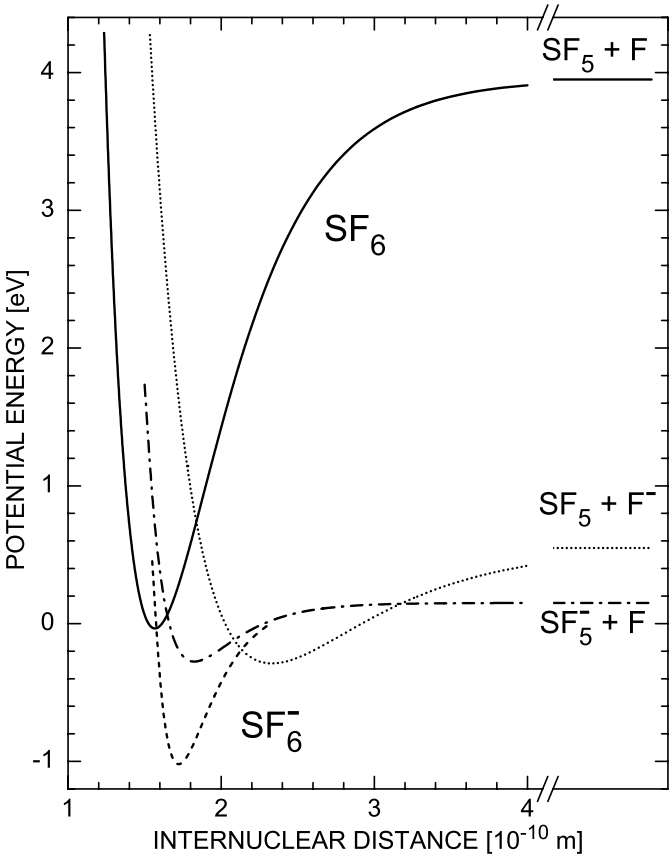

Fig. 8. Simplified potential curve diagram illustrating two different electron attachment paths for SF_5^- formation in low-energy electron collisions with SF_6 molecules, proceeding through capture from the neutral ground state (full curve) into the anion ground state (broken curve) through a virtual state mechanism (zero-energy resonance) and to a repulsive potential surface (chain curve; peak at higher electron energy, around 600 meV at $T_0 = 300$ K). The dotted anion potential is needed to explain F^- formation at higher electron energies, see also text.

strongly with temperature for $T_0 > 400$ K and a broad peak at higher energies whose maximum position shifts towards lower electron energies with rising temperature. The valley between the two peaks fills up with rising temperature and disappears at temperatures above 500 K. At $T_0 = 300$ K the ratio $Y(SF_5^-)/Y(SF_6^-)$ rises slowly with increasing electron energy by a factor of about 2.5 from 2 meV to 200 meV; the minimum of the cross-section for formation of SF_5^- is located at about 200 meV with a yield almost 100 times lower than that in the peak at higher energy (located at about 600 meV, distinctly higher than in most of the previous work). The *shape* of this peak at energies above 600 meV is nearly independent of temperature, and — for energies ≥ 1 eV — it agrees very well with the energy dependence of the cross-section recommended in [2]. In agreement with observations of Chen and Chantry (Fig. 1 in [12]) our data indicate that the *size* of the cross-section in this energy range is essentially independent of temperature.

As compared to the SF_6^- spectra in Figure 5, the SF_5^- attachment spectra in Figure 7 suggest that SF_5^- formation proceeds along two different pathways (see also the discussion in [12,46]):

(i) at low electron energies, the primary attachment occurs through the zero energy capture resonance (responsible for production of metastable SF_6^- ions by intramolecular vibrational redistribution IVR), followed by dissociation into SF_5^- + F(^{2}P);
(ii) at higher energies, the electron is captured into a resonance with a repulsive potential surface on which prompt dissociation towards SF_5^- + F(^{2}P) takes place.

This two-path scheme is illustrated by the schematic potential curve diagram in Figure 8 (a similar diagram has been shown in previous work [46]). We use Morse

potentials to describe the four potential energy curves which have to be viewed as a simplified representation of the relevant potential surfaces. As input we took information provided in [2,46,66–71]. The neutral SF_6 molecule (full curve) and the SF_6^- anion (broken curve) in their respective ground state have octahedral symmetry with S–F equilibrium distances of 156 pm and 172 pm. Symmetry is broken when the systems dissociate into $SF_5 + F$ and $SF_5^- + F$ or $SF_5 + F^-$, respectively. The two lowest anion potential curves in Figure 8 (broken and chain curves, respectively) may be viewed as two different branches of the SF_6^- ground state surface. The lowest (octahedral) anion potential (adopted adiabatic electron affinity 1.0 eV) actually turns into a virtual state which is decisive for electron scattering and attachment at very low energies [58]. The higher-lying asymmetric ($SF_5^- + F$) anion state (dotted curve) mediates dissociative electron attachment via a repulsive potential surface (whose asymptotic energy lies about 0.15 eV above the SF_6 ground state [46,47]). Initial vibrational excitation of SF_6 lowers the vertical attachment energy and leads to the characteristic changes in the SF_5^- attachment spectrum with rising molecular temperature.

As compared to previous work on the energy-dependent yield for SF_5^- formation [2,10–18], our results show the clearest separation between the zero energy peak and the peak at higher energy. In much of the earlier work [10,12–17] the maximum of the higher energy peak was reported to be located between 0.3 and 0.4 eV. Our result is closest to the observation of Brion (maximum located at 0.53(4) eV, see Fig. 1 in [11]). We explain these differences (at least in part) by different internal (vibrational) energies of the SF_6 molecules. In electron beam experiments with a hot cathode as electron source the target chamber will be at a temperature higher than 300 K; moreover, it is possible that the target has a hotter component due to molecules which originate from hotter surfaces close to the cathode and make their way to the reaction volume. Even a small fraction of hotter SF_6 molecules can make a significant contribution to the SF_5^- signal at low electron energies because of the strong rise of the low energy cross-section with gas temperature.

We emphasize that the SF_6 molecules in our supersonic beam possess an effective vibrational temperature which is lower than the nozzle temperature by about 100 K at the lowest stagnation pressure of $p_0 = 1$ bar, as concluded from the comparison of the $T_0 = 400$ K spectrum in Figure 7 with recent data which we obtained with a modified EXLPA method using a static, thermal SF_6 target with $T_i = 300$ K (see Sect. 3.1).

With rising stagnation pressure, the SF_6 molecules in the seeded supersonic beam are progressively cooled to lower temperature T_i. This effect is demonstrated in Figure 9 in which EXLPA spectra for SF_5^- formation at the fixed nozzle temperature $T_0 = 500$ K are compared for the four stagnation pressures 1, 2, 3, and 5 bar. At electron energies above 0.15 eV the shape of the spectrum observed at $T_0 = 500$ K and $p_0 = 5$ bar agrees with that observed at $T_0 = 400$ K and $p_0 = 1$ bar. Since the latter agrees

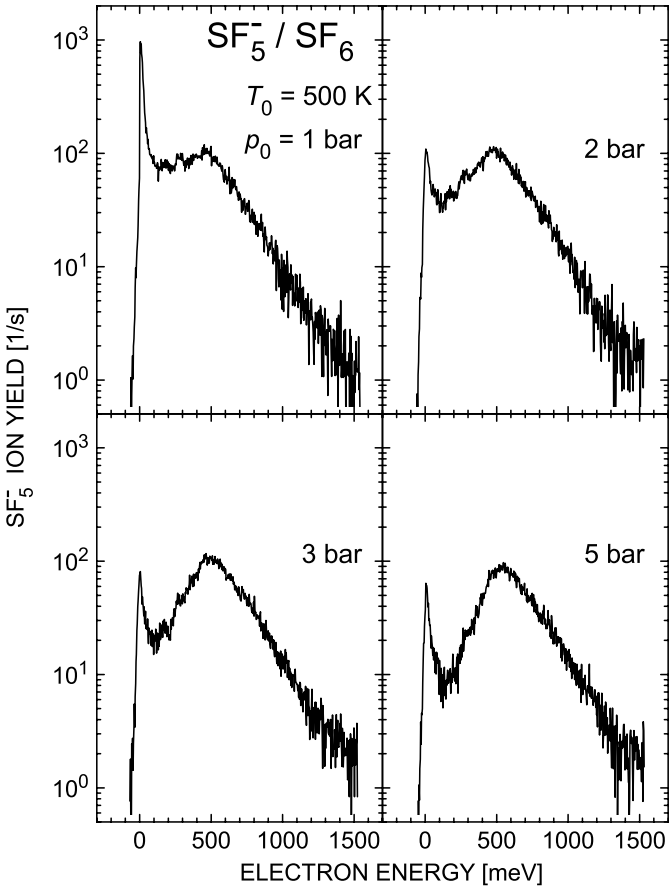

Fig. 9. Energy-dependent yield for SF_5^- formation measured with the EXLPA method at the fixed nozzle temperature $T_0 = 500$ K for the four different stagnation pressures $p_0 = 1$, 2, 3, 5 bar. The changes in the spectra clearly illustrate the reduction of the internal temperature of the SF_6 molecules with rising pressure. The shown anion yields reflect the measured signals without an attempt to correct for possible changes in target density.

with the SF_5^- spectrum observed for a diffuse SF_6 target at 300 K, the use of 5 bar at $T_0 = 500$ K pressure reduces the molecular temperature by about 200 K.

3.5 Attachment spectra for F^- formation

In the course of the present experiments weak signals corresponding to F^- formation were reproducibly observed which we attribute to the process

$$e^-(E) + SF_6 \rightarrow SF_6^{-*} \rightarrow SF_5 + F^-. \qquad (7)$$

The detection of process (7) at near-zero electron energies has been previously reported at experimental energy widths above 0.1 eV and signal levels ≤ 1 % relative to that for SF_6^- [11,22,72], but these observations were questioned in [12,18].

Figure 10 shows F^- attachment spectra recorded with the LPA method at $p_0 = 2$ bar for different nozzle temperatures T_0 in the electron energy range 1.7–200 meV

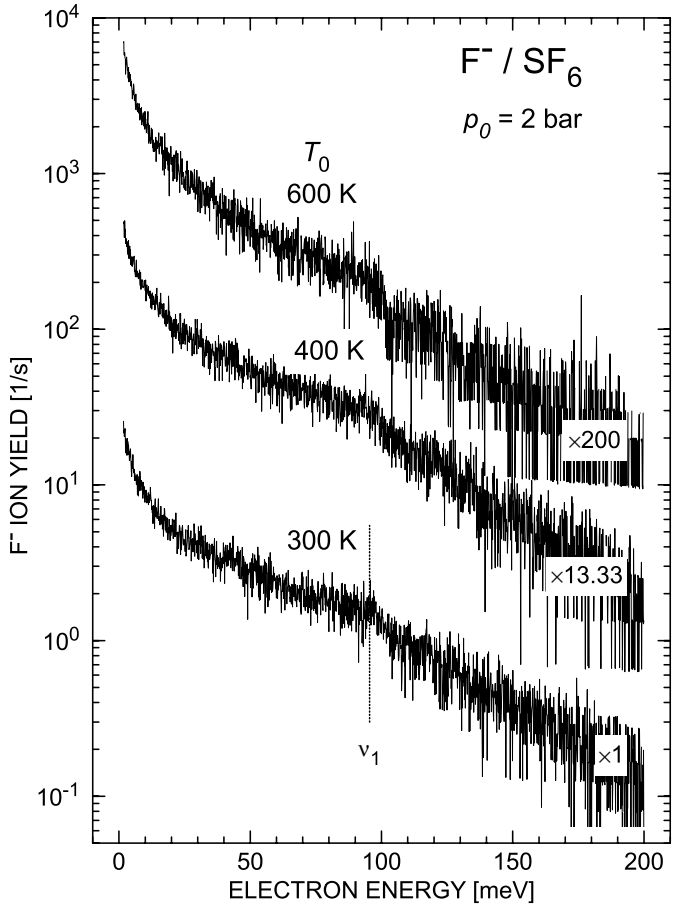

Fig. 10. Attachment spectra for F^- formation measured with a seeded supersonic beam of 12.5% SF_6 in He at $p_0 = 2$ bar for the three nozzle temperatures $T_0 = 300$, 400, 600 K. For clarity, the different data traces have been displaced by the indicated factors (which include the correction for the expected density dependence on nozzle temperature).

(similar data with poorer statistics were obtained at $p_0 = 1$ bar). The energy dependence of these spectra is similar to that observed for SF_6^- formation; correspondingly, the ratios $Y(F^-)/Y(SF_6^-)$ vary rather little: at the two nozzle temperatures $T_0 = 300/600$ K, the ratio increases with rising electron energy from about $1.8 \times 10^{-4}/3 \times 10^{-4}$ at near-zero energy to about $5 \times 10^{-4}/10^{-3}$ at $E = 200$ meV.

It appears that the primary attachment process for reaction (7) is the same as that for SF_6^- production, namely formation of a temporary highly vibrationally excited SF_6^{-*} anion. The increase of the F^-/SF_6^- branching ratio with rising temperature and increasing electron energy may be attributed to the energetics of F^- formation which — based on the value $D_0(SF_5{-}F) = 3.95(14)$ eV [66] for the dissociation energy of SF_6 and on the accurately known electron affinity of the F atom (3.4012 eV [70]) — is endothermic at low internal temperature by about 0.55 eV. We note that a reanalysis of earlier data by Tsang and Herron [73] yielded a recommended value $D_0(SF_5{-}F) = 4.35(10)$ eV at $T_i = 298$ K (see also the results of recent quantum chemistry calculations [74]). This value for the dissociation energy of SF_6 into $SF_5 + F$ implies an endothermicity of 0.95 eV for F^- formation. If this value is indeed correct it is hard to rationalize that F^- anions due to process (7) are observed at low electron energies and molecular temperatures near 300 K (even at the 10^{-4} intensity level relative to the SF_6^- signal).

One may argue that the weak observed F^- signals could be of spurious origin via collision-induced dissociation (CID) of the dominant SF_6^- anion into $SF_5 + F^-$ on the path through the ion optics or within the quadrupole mass spectrometer. Using similar arguments as those presented in the discussion of possible CID contributions to the SF_5^- signals at $T_0 = 300$ K and electron energies below 0.1 eV (see Sect. 3.1) and absolute cross-sections for F^- production in $SF_6^- + SF_6$ collisions from [53], one arrives at the conclusion that CID contributions to the observed F^- signals are possible, but unfortunately they cannot be quantified because the SF_6 density in the region of interest is not sufficiently well-known. The fact that the observed F^-/SF_6^- ratios depend on electron energy indicates that a substantial fraction of the F^- signals is not due to CID involving primary SF_6^- anions. One may imagine scenarios, though, which might explain an energy-dependent rise of the F^-/SF_6^- ratios through the effects of SF_6^- lifetimes in conjunction with CID production of the F^- ions.

Independent information on possible CID contributions to the F^- signal at near-zero electron energy comes from a recent EXLPA study of anion formation from a diffuse SF_6 target at $T_i = 300$ K [50]: when the target density in the reaction chamber was raised from about 1.4×10^{10} cm^{-3} to 8×10^{10} cm^{-3} the ratio $Y(F^-)/Y(SF_6^-)$ (measured at near-zero electron energy) increased from a value of about 3×10^{-4} at the lower density by 23%, pointing to a possible CID contribution of no more than 19% at the higher density. In view of the rather high endothermicity of F^- formation in process (7) the question remains how to explain the majority of the F^- signal observed in this experiment at $T_i = 300$ K and near-zero electron energy. One obvious possible cause are impurities in the SF_6 sample (used in the present and the more recent experiment [50]) which allow F^- formation through an efficient s-wave process. We note that in the positive ion mass spectrum due to 70 eV electron impact we observed impurity ions at m/q values of 35 u/e and 54 u/e which we tentatively attribute to FO^+ and F_2O^+. To clarify this important issue, we plan to carry out experiments with SF_6 samples of higher purity.

4 Conclusions

Using two variants of the laser photoelectron attachment method involving a differentially-pumped, seeded supersonic beam (0.05% and 12.5% of SF_6 molecules in helium carrier gas, nozzle temperatures $T_0 = 300$–600 K, stagnation pressures $p_0 = 1$–5 bar) and mass spectrometric ion detection, we have investigated the energy dependence of

anion formation (SF_6^-, SF_5^-, and F^-) in low-energy electron collisions with SF_6 molecules at high energy resolution. The SF_5^-/SF_6^- intensity ratio at low electron energies as well as the shape of the SF_5^- attachment spectrum at energies above 0.2 eV have been used as thermometers for the internal (vibrational) temperature T_i of the SF_6 molecules in the seeded supersonic beam; the values of T_i are found to be 50–200 K below the nozzle temperature T_0 in the covered ranges for p_0 and T_0.

The cross-section for formation of SF_6^- decreases by five orders of magnitude over the range 1–500 meV and is only weakly dependent on nozzle temperature. Our results indicate that SF_6^- anions formed in free electron attachment at temperatures T_i around 300 K and low electron energies ($\leq$90 meV) have autodetachment lifetimes not far from those for SF_6^- anions due to Rydberg electron attachment at high principal quantum numbers. Since the latter are at least 300 μs [5,30,31] (and more likely several ms [33]) our results do not support the findings in [32] where a lifetime close to 20 μs was reported for SF_6^- anions formed by attachment of photoelectrons with energies 1–100 meV to SF_6 molecules in a pulsed supersonic beam.

The yield for SF_5^- formation shows — apart from a weak zero energy peak which grows strongly with rising temperature — a broad maximum (located around 0.55 eV for $T_0 = 400$ K which corresponds to a molecular temperature of about 300 K) and a monotonical decrease towards higher energies. SF_5^- attachment spectra taken at elevated temperatures exhibit changes with rising stagnation pressure which directly reflect rovibrational cooling of the SF_6 molecules with rising pressure. The present results offer a consistent picture of the qualitative effects of the internal SF_6 energy on SF_6^- and SF_5^- formation over the electron energy range 1–1500 meV. To gain further insight, it is desirable to measure the attachment spectra for SF_6^- and SF_5^- formation at well defined values of T_i with narrow energy widths and to provide absolute partial cross-sections. Moreover, lifetime measurements of SF_6^- as a function of temperature T_i and electron energy E are of great interest.

The energy dependence of the yield for F^- formation is similar to that for SF_6^-, but the F^- signals are three to four orders of magnitude lower than those for SF_6^-. In view of the rather high endothermicity of F^- formation (at least 0.55 eV) spurious sources for the F^- signals (impurities in the SF_6 sample and collision-induced dissociation (CID) of the abundant primary SF_6^- yielding F^- ions) have to be carefully considered. While CID contributions are probably weak, impurities may be more important; in the future we plan to carry out experiments with SF_6 samples of higher purity.

This work has been supported by the Deutsche Forschungsgemeinschaft and by the Forschungszentrum OTLAP. We gratefully acknowledge I.I. Fabrikant for several helpful discussions and T.M. Miller for valuable comments on the manuscript. We thank U. Buck for a discussion on seeded supersonic beams and for estimating the velocity slip in our mixed He–SF_6 beams.

References

1. *Electron molecule interactions and their applications*, edited by L.G. Christophorou (Academic Press, New York 1984), Vol. 1 and 2
2. L.G. Christophorou, J.K. Olthoff, J. Phys. Chem. Ref. Data **29**, 267 (2000)
3. E.P. Wigner, Phys. Rev. **73**, 1002 (1948)
4. A. Chutjian, S.H. Alajajian, Phys. Rev. A **31**, 2885 (1985)
5. D. Klar, M.-W. Ruf, H. Hotop, Chem. Phys. Lett. **189**, 448 (1992); D. Klar, M.-W. Ruf, H. Hotop, Austr. J. Phys. **45**, 263 (1992)
6. F.B. Dunning, J. Phys. B **28**, 1645 (1995)
7. A. Schramm, J.M. Weber, J. Kreil, D. Klar, M.-W. Ruf, H. Hotop, Phys. Rev. Lett. **81**, 778 (1998)
8. P.-T. Howe, A. Kortyna, M. Darrach, A. Chutjian, Phys. Rev. A **64**, 042706 (2001)
9. H. Hotop, M.-W. Ruf, M. Allan, I.I. Fabrikant, Adv. At. Mol. Opt. Phys. **49**, 85 (2003)
10. W.M. Hickam, R.E. Fox, J. Chem. Phys. **25**, 642 (1956)
11. C.E. Brion, Int. J. Mass Spectr. Ion Phys. **3**, 197 (1969)
12. C.L. Chen, P.J. Chantry, J. Chem. Phys. **71**, 3897 (1979)
13. L.E. Kline, D.K. Davies, C.L. Chen, P.J. Chantry, J. Appl. Phys. **50**, 6789 (1979)
14. R.N. Compton, in *Electronic and Atomic Collisions*, edited by N. Oda, K. Takayanagi (North Holland Publ. Co., 1980), p. 251f
15. S.R. Hunter, J.G. Carter, L.G. Christophorou, J. Chem. Phys. **90**, 4879 (1989)
16. D. Smith, P. Spaněl, S. Matejcik, A. Stamatovic, T.D. Märk, T. Jaffke, E. Illenberger, Chem. Phys. Lett. **240**, 481 (1995)
17. A. Rosa, F. Brüning, S.V.K. Kumar, E. Illenberger, Chem. Phys. Lett. **391**, 361 (2004)
18. M. Fenzlaff, R. Gerhard, E. Illenberger, J. Chem. Phys. **88**, 149 (1988)
19. D. Edelson, J.E. Griffiths, K.B. McAfee Jr, J. Chem. Phys. **37**, 917 (1962)
20. R.N. Compton, L.G. Christophorou, G.S. Hurst, P.W. Reinhardt, J. Chem. Phys. **45**, 4634 (1966)
21. J.M.S. Henis, C.A. Mabie, J. Chem. Phys. **53**, 2999 (1970)
22. P.W. Harland, J.C.J. Thynne, J. Phys. Chem. **75**, 3517 (1971)
23. R.W. Odom, D.L. Smith, J.H. Futrell, J. Phys. B **8**, 1349 (1975)
24. M.S. Foster, J.L. Beauchamp, Chem. Phys. Lett. **31**, 482 (1975)
25. J.P. Astruc, R. Barbé, A. Lagrèze, J.P. Schermann, Chem. Phys. **75**, 405 (1983)
26. M. Vedel, J. André, G. Brincourt, Y. Zerega, G. Werth, J.P. Schermann, Appl. Phys. B **34**, 229 (1984)
27. J.E. Delmore, A.D. Appelhans, J. Chem. Phys. **84**, 6238 (1986)
28. A.D. Appelhans, J.E. Delmore, J. Chem. Phys. **88**, 5561 (1988)
29. G. Brincourt, S. Rajab Pacha, R. Catella, Y. Zerega, J. André, Chem. Phys. Lett. **156**, 573 (1989)
30. R.A. Popple, M.A. Durham, R.W. Marawar, B.G. Lindsay, K.A. Smith, F.B. Dunning, Phys. Rev. A **45**, 247 (1992)
31. C.D. Finch, R. Parthasarathy, S.B. Hill, F.B. Dunning, J. Chem. Phys. **111**, 7316 (1999)
32. J.-L. Le Garrec, D.A. Steinhurst, M.A. Smith, J. Chem. Phys. **114**, 8831 (2001)

33. L. Suess, R. Parthasarathy, F.B. Dunning, J. Chem. Phys. **117**, 11222 (2002); Y. Liu, L. Suess, F.B. Dunning, J. Chem. Phys. **122**, 214313 (2005)
34. D. Klar, M.-W. Ruf, H. Hotop, Meas. Sci. Technol. **5**, 1248 (1994)
35. A. Schramm, I.I. Fabrikant, J.M. Weber, E. Leber, M.-W. Ruf, H. Hotop, J. Phys. B **32**, 2153 (1999)
36. J.M. Weber, E. Leber, M.-W. Ruf, H. Hotop, Eur. Phys. J. D **7**, 587 (1999)
37. I.D. Petrov, V.L. Sukhorukov, E. Leber, H. Hotop, Eur. Phys. J. D **10**, 53 (2000)
38. A. Gopalan, E. Leber, J. Bömmels, S.P.H. Paul, M. Allegrini, M.-W. Ruf, H. Hotop, Eur. Phys. J. D **30**, 163 (2004)
39. J. Bömmels, E. Leber, A. Gopalan, J.M. Weber, S. Barsotti, M.-W. Ruf, H. Hotop, Rev. Scient. Instrum. **72**, 4098 (2001)
40. H. Hotop, D. Klar, J. Kreil, M.-W. Ruf, A. Schramm, J.M. Weber, in *The Physics of Electronic and Atomic Collisions*, edited by L.J. Dubé, J.B.A. Mitchell, J.W. McConkey, C.E. Brion, AIP Conf. Proc. No. **360** (AIP Press, Woodbury, NY, 1995), p. 267
41. D.R. Miller, in *Atomic and Molecular Beam Methods*, edited by G. Scoles (Oxford Univ. Press, New York, 1988), Chap. 2, p. 14ff
42. U. Buck, private communication (2002)
43. H.S.W. Massey, *Negative Ions* (Cambridge University Press, London, 1976)
44. F.C. Fehsenfeld, J. Chem. Phys. **53**, 2000 (1970)
45. T.M. Miller, A.E. Stevens, J.F. Paulson, X. Liu, J. Chem. Phys. **100**, 8841 (1994)
46. E.C.M. Chen, L.-R. Shuie, E.D. D'sa, C.F. Batten, W.E. Wentworth, J. Chem. Phys. **88**, 4711 (1988)
47. P. Spanel, S. Matejcik, D. Smith, J. Phys. B **28**, 2941 (1995)
48. A. Schramm, Dissertation, Fachbereich Physik, Univ. Kaiserslautern, Shaker Verlag (Aachen, 1998), ISBN 3-8265-3657-6
49. J.M. Weber, M.-W. Ruf, H. Hotop, Z. Phys. D **37**, 351 (1996)
50. M. Braun, S. Marienfeld, M.-W. Ruf, H. Hotop, J. Phys. B (in preparation)
51. T. Kraft, M.-W. Ruf, H. Hotop, in *Electronic and Atomic Collisions*, edited by W.R. MacGillivray, I.E. McCarthy, M.C. Standage (Bristol, Philadelphia, New York, 1992), p. 599
52. E.E. Ferguson, Int. J. Mass Spectr. Ion Proc. **19**, 53 (1976)
53. Y. Wang, R.L. Champion, L.D. Doverspike, J.K. Olthoff, R.J. van Brunt, J. Chem. Phys. **91**, 2254 (1989)
54. D. Klar, B. Mirbach, H.J. Korsch, M.-W. Ruf, H. Hotop, Z. Phys. D **31**, 235 (1994)
55. D. Spence, G.J. Schulz, J. Chem. Phys. **58**, 1800 (1973)
56. D. Smith, N.G. Adams, E. Alge, J. Phys. B **17**, 461 (1984)
57. Z.L. Petrovic, R.W. Crompton, J. Phys. B **18**, 2777 (1985)
58. J.L. Le Garrec, O. Sidko, J.L. Queffelec, S. Hamon, J.B.A. Mitchell, B.R. Rowe, J. Chem. Phys. **107**, 54 (1997)
59. I.I. Fabrikant, M. Allan, H. Hotop, Phys. Rev. A **71**, 022712 (2005)
60. D. Field, N.C. Jones, J.-P. Ziesel, Phys. Rev. A **69**, 052716 (2004)
61. J.P. Gauyacq, A. Herzenberg, J. Phys. B **17**, 1155 (1984)
62. F.B. Dunning, J. Phys. Chem. **91**, 2244 (1987)
63. C.E. Klots, Chem. Phys. Lett. **38**, 61 (1976)
64. D. Klar, Dissertation, Fachbereich, Univ. Kaiserslautern (1993), unpublished
65. I.I. Fabrikant, private communication (2005)
66. T. Kiang, R.N. Zare, J. Am. Chem. Soc. **102**, 4024 (1980)
67. L.M. Babcock, G.E. Streit, J. Chem. Phys. **74**, 5700 (1981)
68. C.L. Lugez, M.E. Jacox, R.A. King, H.F. Schaefer III, J. Chem. Phys. **108**, 9639 (1998)
69. B.L. Gutsev, R.J. Bartlett, Mol. Phys. **94**, 121 (1998)
70. T. Andersen, H. Haugen, H. Hotop, J. Phys. Chem. Ref. Data **28**, 1511 (1999)
71. S.V.K. Kumar, Abstracts of *Int. Symposium on Electron-Molecule Collisions and Swarms* (EMS-03), p. 141, Pruhonice, Prague, Czech Republic (2003)
72. R.K. Curran, J. Chem. Phys. **34**, 1069 (1961)
73. W. Tsang, J.T. Herron, J. Chem. Phys. **96**, 4272 (1992)
74. T.M. Miller, S.T. Arnold, A.A. Viggiano, Int. J. Mass Spectr. **227**, 413 (2003)